

UCSF

UC San Francisco Previously Published Works

Title

CD94+ Natural Killer cells potentiate pulmonary ischemia-reperfusion injury.

Permalink

<https://escholarship.org/uc/item/01z0v5rx>

Journal

European Respiratory Journal, 64(3)

ISSN

0903-1936

Authors

Tsao, Tasha

Qiu, Longhui

Bharti, Reena

et al.

Publication Date








2024-08-01

DOI

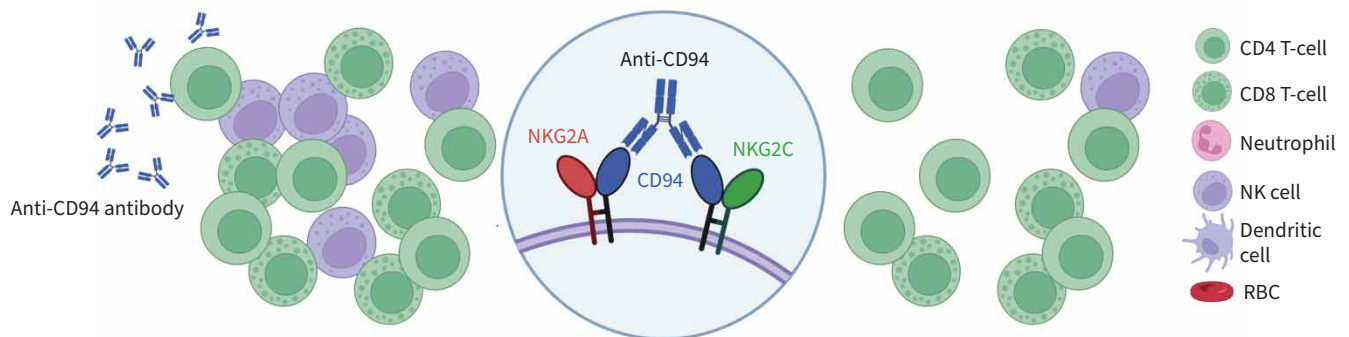
10.1183/13993003.02171-2023

Peer reviewed

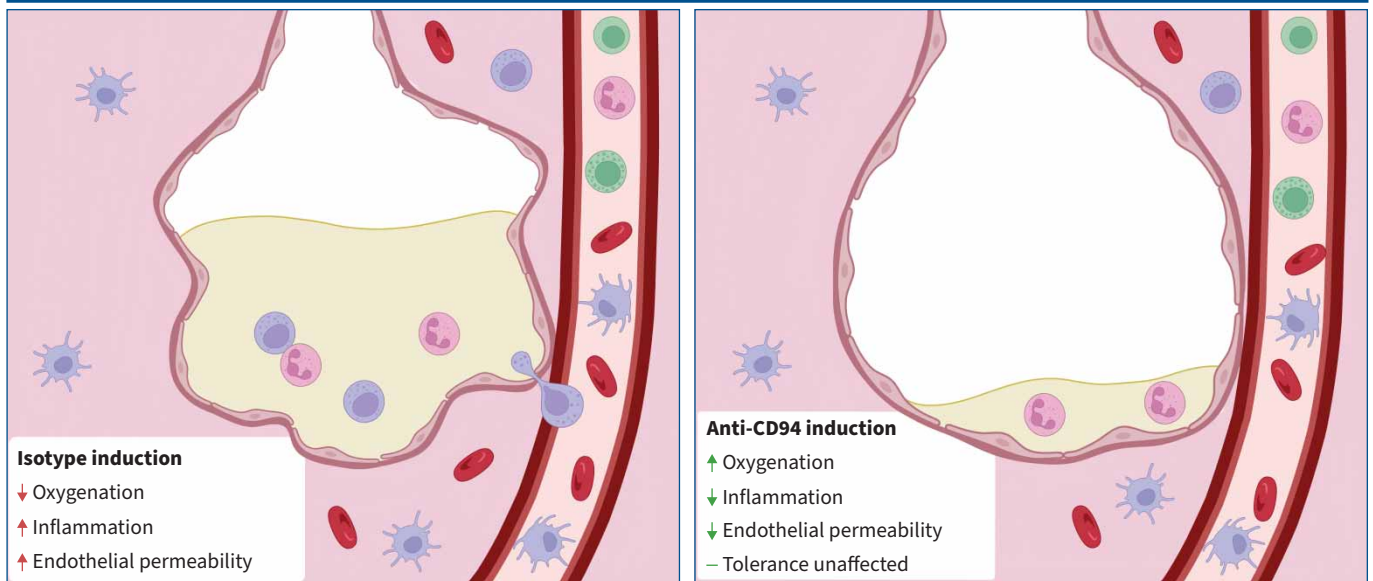
CD94⁺ natural killer cells potentiate pulmonary ischaemia–reperfusion injury

Tasha Tsao , Longhui Qiu, Reena Bharti, Avishai Shemesh, Alberto M. Hernandez, Simon J. Cleary , Nancy Y. Greenland, Jesse Santos, Ruoshi Shi, Lu Bai, Jennifer Richardson, Kimberley Dilley, Matthias Will, Nenad Tomasevic, Tereza Sputova, Adam Salles, Jeffrey Kang, Dongliang Zhang, Steven R. Hays , Jasleen Kukreja, Jonathan P. Singer , Lewis L. Lanier, Mark R. Looney , John R. Greenland  and Daniel R. Calabrese 

Anti-CD94 monoclonal antibodies target mouse and human NK cells for depletion



Lung ischaemia–reperfusion injury



GRAPHICAL ABSTRACT Overview of the study. NK: natural killer; RBC: red blood cell.



CD94⁺ natural killer cells potentiate pulmonary ischaemia–reperfusion injury

Tasha Tsao ^{1,10}, Longhui Qiu^{1,10}, Reena Bharti¹, Avishai Shemesh^{1,2}, Alberto M. Hernandez^{2,3}, Simon J. Cleary ⁴, Nancy Y. Greenland⁵, Jesse Santos⁶, Ruoshi Shi⁷, Lu Bai⁷, Jennifer Richardson⁷, Kimberley Dilley⁷, Matthias Will⁷, Nenad Tomasevic⁷, Tereza Sputova⁷, Adam Salles⁷, Jeffrey Kang⁷, Dongliang Zhang¹, Steven R. Hays ¹, Jasleen Kukreja⁸, Jonathan P. Singer ¹, Lewis L. Lanier^{2,3}, Mark R. Looney ¹, John R. Greenland ^{1,9} and Daniel R. Calabrese ^{1,9}

¹Department of Medicine, University of California San Francisco, San Francisco, CA, USA. ²Parker Institute for Cancer Immunotherapy San Francisco, San Francisco, CA, USA. ³Department of Microbiology and Immunology, University of California San Francisco, San Francisco, CA, USA. ⁴Institute of Pharmaceutical Science, King's College London, London, UK. ⁵Department of Pathology, University of California San Francisco, San Francisco, CA, USA. ⁶Department of Surgery, University of California San Francisco – East Bay, Oakland, CA, USA. ⁷Dren Bio, Foster City, CA, USA. ⁸Department of Surgery, University of California San Francisco, San Francisco, CA, USA. ⁹Medical Service, Veterans Affairs Health Care System, San Francisco, CA, USA. ¹⁰T. Tsao and L. Qiu contributed equally.

Corresponding author: Daniel R. Calabrese (daniel.calabrese@ucsf.edu)



Shareable abstract (@ERSpublications)

Pulmonary ischaemia–reperfusion injury accounts for significant morbidity after lung transplant but has no known medical therapies. This study identified a critical role for the natural killer cell co-receptor CD94 in mouse and human lung transplant. <https://bit.ly/3WdSghb>

Cite this article as: Tsao T, Qiu L, Bharti R, *et al.* CD94⁺ natural killer cells potentiate pulmonary ischaemia–reperfusion injury. *Eur Respir J* 2024; 64: 2302171 [DOI: 10.1183/13993003.02171-2023].

Copyright ©The authors 2024.
For reproduction rights and
permissions contact
permissions@ersnet.org

Received: 4 Dec 2023
Accepted: 30 June 2024

Abstract

Background Pulmonary ischaemia–reperfusion injury (IRI) is a major contributor to poor lung transplant outcomes. We recently demonstrated a central role of airway-centred natural killer (NK) cells in mediating IRI; however, there are no existing effective therapies for directly targeting NK cells in humans.

Methods We hypothesised that a depleting anti-CD94 monoclonal antibody (mAb) would provide therapeutic benefit in mouse and human models of IRI based on high levels of *KLRD1* (CD94) transcripts in bronchoalveolar lavage samples from lung transplant patients.

Results We found that CD94 is highly expressed on mouse and human NK cells, with increased expression during IRI. Anti-mouse and anti-human mAbs against CD94 showed effective NK cell depletion in mouse and human models and blunted lung damage and airway epithelial killing, respectively. In two different allogeneic orthotopic lung transplant mouse models, anti-CD94 treatment during induction reduced early lung injury and chronic inflammation relative to control therapies. Anti-CD94 did not increase donor antigen-presenting cells that could alter long-term graft acceptance.

Conclusions Lung transplant induction regimens incorporating anti-CD94 treatment may safely improve early clinical outcomes.

Introduction

Lung transplantation is a life-prolonging therapy for patients with advanced lung disease [1]. However, the potential benefit of lung transplant is hampered by early ischaemia–reperfusion injury (IRI) [2]. Severe IRI manifests clinically as primary graft dysfunction (PGD), defined as diffuse bilateral pulmonary opacities on imaging and hypoxaemia during day 2 or 3 following transplantation [3]. PGD is a multifaceted disease that occurs in up to a third of all lung transplant recipients, drives 50% of the first-year mortality, is associated with poor quality of life and chronic rejection, and is increasing in incidence [4–8]. Like other acute lung injury syndromes, PGD has no medical therapies known to be effective for prevention or improvement of injury.

The pathophysiology of IRI results from a cascade of events initiated with endothelial and epithelial injury leading to inflammatory mediator release and graft infiltration by innate immune cells [9]. We have

described a central role for natural killer (NK) cells in mediating the early injury of IRI [10]. NK cells are innate immune cells with the primary function to surveil for missing, damaged or transformed self [11]. In contrast to B- and T-cells, where antigen specificity is dependent upon genetic rearrangement, NK cell actions are determined by the integration of a myriad of somatically encoded inhibitory or activating receptors [10]. In experimental models of IRI and in human PGD samples, we identified that NK cell activation occurs *via* recognition of stress molecules on the surfaces of epithelial and endothelial cells through the NKG2D receptor [12–14]. Moreover, NK cell depletion or NKG2D blockade blunted lung injury *in vitro* and *in vivo*.

Lung transplant recipients can receive a variety of immunosuppression agents throughout the life of the allograft [15]. Pertinent to PGD, many centres give induction regimens that contain corticosteroids, anti-thymocyte globulin, calcineurin inhibitors, cell cycle inhibitors or interleukin (IL)-2 receptor blockade [16]. Notably, NK cells are resistant to many of these agents as they are resident in the graft and thus difficult to expose to therapeutic drug concentrations. Moreover, their effector functions are not dependent upon transcription as they store their effector molecules in pre-formed cytoplasmic granules [17]. In fact, IL-2 receptor blockade may lead to NK cell activation through secondary scavenging of IL-2 [18]. mTOR inhibition dampens NK cell function but cannot be given early after lung transplant due to issues with anastomotic healing [19, 20]. To date, there are no NK cell-specific therapies available for direct depletion or broad receptor inhibition in humans.

Mouse and human NK cells have many homologous receptors, co-receptors and adapter molecules [21]. While NK cell depletion targeting the NK1.1 receptor results in efficient depletion of mouse NK cells, there has not yet been a successful approach in effecting human NK cell depletion, and the human orthologue of NK1.1 (CD161) is not expressed by all NK cells [13, 22]. Moreover, targeting NK cells *via* NKG2D receptor blockade in inflammatory bowel disease did not result in clinically meaningful differences in outcomes in most patients [23]. Thus, there is need for an alternate and broader NK cell-targeted approach. Here, we sought to identify a novel target for NK cell subset depletion. We hypothesised that a mAb against a cell surface protein preferentially expressed on all NK cells, but only a minor subset of T-cells, would efficiently deplete NK cells in the mouse lung and human blood cells and would blunt injury in mouse experimental and human *in vitro* models of IRI.

Methods

Mice

Male C57BL/6J (000664), BALB/cJ (000651) and C57BL/6J CD45.1 (B6.SJL-*Ptprc*^a *Pepc*^b/BoyJ; 002014) mice weighing 25–30 g were purchased from Jackson Laboratories. B6.C-*H2*^d/bByJ (B6.H2^d; 000359) mice originated from Jackson Laboratories and were bred and maintained at the University of California San Francisco (UCSF) [24]. Mice were housed in a pathogen-free barrier facility and experiments were conducted according to protocols approved by the UCSF Institutional Animal Care Use Committee.

Experimental models of lung IRI and lung transplantation

Warm IRI was performed by an experienced microvascular surgeon as previously described [13, 25, 26]. After anaesthetisation, mice underwent a left thoracotomy, then a slipknot suture was tied around the left hilum (hilar clamp (HC)) or left untied as a sham surgery. The suture was removed after 2 h of ischaemia and animals were euthanised after 4 h of reperfusion. Mice were treated 24 h preceding IRI surgery with 10 mg·kg⁻¹ of anti-mouse anti-CD94 antibody (Dren Bio) or 10 mg·kg⁻¹ of anti-mouse IgG2a isotype-matched control (Clone C1.18.4; Bio X Cell; BP0085). Single left lung bronchoalveolar lavage (BAL) was performed by gently lavaging 300 µL of PBS. BAL, bilateral lungs and blood were collected for analysis.

We also performed allogeneic orthotopic lung transplantation with minimal warm ischaemia (OLT-MWI) without immunosuppression to assess the chronic rejection of obliterative airway disease [27]. Left BALB/c donor lungs were procured and transplanted into C57BL/6 or C57BL/6 CD45.1 recipient mice using interrupted sutures for the anastomoses. Recipient mice received 10 mg·kg⁻¹ of anti-mouse anti-CD94 antibody (Dren Bio), 10 mg·kg⁻¹ of anti-mouse IgG2a isotype-matched control (Clone C1.18.4; Bio X Cell; BP0085) or 0.4 mg·kg⁻¹ of IL-15/IL-15 receptor complex (IL-15RC) 1 h before OLT-MWI. IL-15 was complexed prior to injection by mixing 1.5 µg of mouse recombinant IL-15 (R&D Systems; 447ML010CF) with 10.05 µg of mouse recombinant IL-15 receptor α -Fc (R&D Systems; 551MR100) and incubated at 37°C for 20 min. As a negative control, we also performed syngeneic orthotopic left lung transplantation from a C57BL/6 donor to a C57BL/6 recipient with MWI (isograft). The recipient animals were euthanised 3 or 14 days after transplantation. The left and right lungs and blood were collected for analysis.

We also performed allogeneic OLT with cold ischaemia (OLT-CI) without immunosuppression to assess IRI in a setting more closely approximating human lung transplantation. Left lungs from B6.H2^d mice, congenic except at the major histocompatibility complex (MHC) locus, were procured, perfused with 1 mL of heparinised saline, covered with a saline-soaked gauze and placed at 4°C for 4 h of CI before being transplanted into C57BL/6 recipient mice using the same surgical method detailed for the allogeneic OLT-MWI. Donor and recipient mice received 10 mg·kg⁻¹ of anti-mouse anti-CD94 antibody (Dren Bio) or 10 mg·kg⁻¹ of anti-mouse IgG2a isotype-matched control (Clone C1.18.4; Bio X Cell; BP0085) 24 h before OLT-CI. The recipient animals were euthanised 20 h after transplantation. The left lung was collected for analysis.

Acute lung injury measurements and lung digestion

We assessed lung vascular permeability to ¹²⁵I-labelled albumin (Jeanotope; Iso-Tex Diagnostics), γ counts of ¹²⁵I-labelled albumin per gram of dried lung and arterial oxygen tension (P_{aO_2}) as previously described [13, 26]. Endothelial permeability was calculated by quantifying the clearance of ¹²⁵I-labelled albumin across the endothelium and into extravascular space as previously described [28, 29]. Lung samples for histopathology were collected in 1% paraformaldehyde (Thermo Fisher; 047392.9M), then stored in 70% ethanol before paraffin embedding, sectioning and haematoxylin/eosin (HE) staining. Slides were scanned with a Zeiss Axio Scan.Z1 microscope and digitally assessed with ImageJ software [30]. Lungs were placed into 1 mL of PBS with 10 μL of 10 μg·μL⁻¹ collagenase D (Sigma-Aldrich; 11088858001) and 10 μL of 10 μg·μL⁻¹ DNase I (10104159001; Sigma-Aldrich), dissociated, and processed as previously described [13].

Anti-mouse anti-CD94 mAb production and purification

The antibody sequence vector and plasmid DNA were constructed using the pCDNA3.4 kit (Thermo Fisher; A14697). Antibody variable light gene and variable heavy gene were cloned into pFUSE2-CLIg-hK (Invivogen; pfuse2-hclk) and pFUSE-CHlg-hG1 (Invivogen; pfusehchg1), respectively (supplementary figure S2a and b). Cloning was done by Genscript. A HEK-293 (Invitrogen) cell line lacking fucosyl transferase (293-NF) was used to produce non-fucosylated antibody. 293-NF and suspension HEK-293 cells were co-transfected with expression plasmid containing genes encoding the heavy chain and the light chain in a 1:1 ratio using an ExpiFectamine 293 Transfection Kit (Thermo Fisher; A14524) according to the manufacturer's recommendations. Cells were collected 5 days after transfection and cell culture fluid was obtained through centrifugation and sterile filtration. Cell culture fluid was purified using a Protein A affinity chromatography column on an AKTA Pure 150 (Cytiva). Protein concentration was determined by UV absorbance at 280 nm. Monomer content was determined by high-performance liquid chromatography size exclusion using a HiLoad Superdex 200 column (Cytiva) (supplementary figure S2c). Glycan distribution across fucosylated and non-fucosylated antibodies was determined with the Glycan Profiling Assay Release Kit (PerkinElmer; CLS155434) (supplementary figure S2d). Binding of the antibody to mouse CD16a and mouse CD94 was measured by biolayer interferometry on an Octet (Sartorius) (supplementary figure S2e). To assess antibody affinity for antigen bound to the cell surface, mouse CD94-transduced Ba/F3 cells were generated (Lewis L. Lanier) [14]. Anti-mouse CD94 antibody was titrated with 3-fold dilutions and incubated with CD94⁺ Ba/F3 cells for 30 min followed by staining with 1:300 dilution of AffiniPure Goat Anti-Mouse IgG, Fcγ fragment specific Alexa Fluor 647 secondary antibody (Jackson ImmunoResearch; 115-605-071). Data were acquired on a CytoFlex LX flow cytometer (Beckman Coulter) and mean fluorescence intensity (MFI) values were obtained with FlowJo (Ashland) (supplementary figure S2f).

BAL protein quantification

BAL fluid was centrifuged at 300×g for 10 min at 4°C to pellet cells. Isolated BAL supernatant was stored at -80°C as recommended by the assay kit manufacturer. Protein quantification was done using a BCA assay kit (Pierce BCA Protein Assay Kit; Thermo Fisher; 23225) according to the manufacturer's instructions.

Cell-free DNA quantification

Blood was collected from mice using EDTA-coated tubes to prevent coagulation. Blood was mixed gently by inverting the tube a few times to ensure thorough mixing with the anticoagulant. Blood collection tubes were centrifuged at 1600×g for 10 min at 4°C to separate the plasma from cellular components. Plasma was collected (top layer) into a 2 mL microcentrifuge tube without disturbing the buffy coat or red blood cell layer and cell-free DNA isolation from blood plasma was done according to the MagMAX Cell-free DNA isolation kit (Thermo Fisher; A29319). Isolated cell-free DNA was quantified using the Qubit dsDNA Assay Kit.

Mouse lung immunophenotyping

Lung cell suspensions were washed and incubated at 37°C with anti-mouse anti-CD16/CD32 (BioLegend; 101320) to block non-specific binding and stained with viability exclusion dye. Cells were further stained with the remaining fluorophore-conjugated antibodies at 4°C and washed. Antibody panels and gating strategies are detailed for four different flow cytometry panels used to: 1) immunophenotype CD94⁺ NK cells at rest (supplementary table S2 and supplementary figure S1), 2) assess NKG2A⁺ NK cells during IRI (supplementary table S3 and supplementary figure S1), 3) quantify NK cells during IRI depletion experiments (supplementary table S4 and supplementary figure S1) and 4) measure donor antigen-presenting cells (APCs) following allogeneic OLT-MWI (supplementary table S5 and supplementary figure S8). Data were acquired on BD Biosciences LSR II and LSR Fortessa flow cytometers. Flow cytometry data were visualised and analysed with FCS express (De Novo Software).

Human in vitro NK cell depletion and airway epithelial cell co-culture experiments

Human samples were collected from consenting adults. Peripheral blood mononuclear cells (PBMCs) from five lung transplant recipients who underwent lung transplantation at the UCSF were obtained within the first year after transplantation. Supplementary table S6 shows baseline characteristics for this cohort. NK cells, CD4 T-cells and CD8 T-cells were quantified with flow cytometry (supplementary table S7) before and after treatment with anti- β -galactosidase human IgG1 isotype-matched control antibody (InvivoGen; bgal-mab13) and anti-human anti-CD94 mAb (Dren Bio) across a range of concentrations from 1×10^{-6} to $10 \mu\text{g} \cdot \text{mL}^{-1}$.

To assess airway epithelial cell cytotoxicity, human bronchial epithelial cells (16HBE14o-; Sigma-Aldrich; SCC150) were plated and allowed to adhere overnight. They were then exposed to hypoxia (1% O₂) for 24 h and co-cultured in a 2:1 effector:target ratio with PBMCs treated with IgG isotype-matched control antibody or anti-CD94 antibody for an additional 24 h. Airway epithelial cells were stained with CellTrace Violet (Invitrogen; C34557) prior to plating to distinguish PBMCs from epithelial cells. Upon collection, cells were stained with Fixable Viability Dye eFluor 660 (Invitrogen; 65-0864-14) and data were collected on a BD FACSAria Fusion flow cytometer.

Human lung transplant BAL RNA sequencing and immunophenotyping

BAL was collected on the first post-transplant day from consenting lung allograft recipients at two centres through a previous study [12]. RNA sequencing was performed on the BAL cell pellet as previously described [12]. Supplementary table S8 shows the baseline characteristics for this cohort, which contains two additional samples from the previously published cohort. All studies of human samples were conducted according to approved institutional review board protocols.

As previously reported, we also collected BAL from lung transplant recipients with severe PGD (n=5) and those without PGD (n=7) within 2 weeks of lung transplantation [25]. Samples from recipients with PGD were matched based on age, sex, transplant indication and ethnicity to no PGD recipient samples. Supplementary table S1 shows the baseline characteristics for the recipients included in these analyses.

Statistical analyses

Experimental data were tested for normality with the Shapiro–Wilk test. Comparisons of means in experiments with multiple groups were made with the Kruskal–Wallis test or ANOVA and *post hoc* differences were assessed with the two-tailed Mann–Whitney U-test or t-test, as appropriate. All tests were adjusted for multiple comparisons with the Benjamini–Hochberg approach. Differences between NK cell surface markers were determined with paired testing. Results were visualised using box-and-whisker plots showing individual data points bound by boxes at the 25th and 75th percentiles and medians depicted with bisecting lines. RNA sequencing NK cell genetic screen was performed with a random forest model using 18 NK cell genes as predictors of severe PGD with leave-one-out validation. The model results were visualised *via* feature plot relative importance and the model's fit was tested with area under the curve of the receiver operator characteristic curve (AUC ROC). A p-value <0.05 was considered significant. Analyses and plotting were performed in R (R Foundation for Statistical Computing).

Study approval

The UCSF Institutional Review Board approved the human subject components of this study under protocol 13–10738. Written informed consent was obtained from all participants prior to inclusion in the study. All animal procedures and experiments were conducted according to protocols approved by the UCSF Institutional Animal Care Use Committee.

Results

Human RNA sequencing screen of PGD BAL cells identifies *KLRD1* (CD94) as a rational NK cell target

BAL was collected on the first post-operative day after lung transplantation and cells from participants with severe PGD (n=20) and those without PGD (n=18) underwent RNA sequencing as previously reported [12]. To identify a plausible marker for NK cell targeting, we performed a genomic screen of 18 NK cell-associated transcripts using a random forest model to predict severe PGD with leave-one-out validation. The model had high sensitivity and specificity (AUC ROC 0.76 (95% CI 0.61–0.91)) with accuracy displayed in a ROC plot (figure 1a). We found that *KLRD1*, encoding the CD94 surface protein, had the highest feature importance across the 18 NK cell genes (figure 1b). We investigated *KLRD1* gene

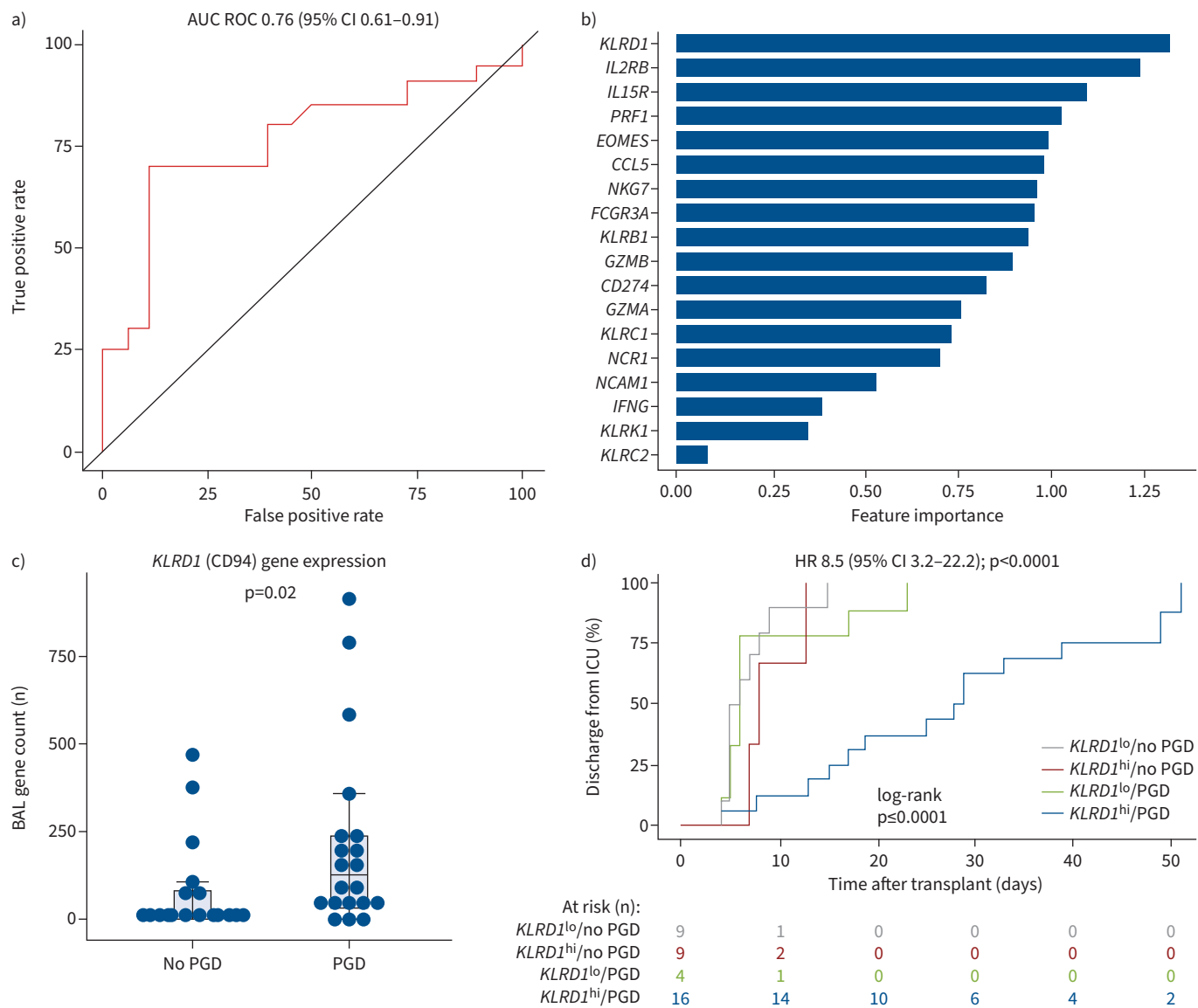


FIGURE 1 Bronchoalveolar lavage (BAL) RNA sequencing screen of potential natural killer (NK) cell targets. RNA sequencing was performed on BAL collected on the first post-operative day after lung transplantation in recipients with severe primary graft dysfunction (PGD) (n=20) and those without PGD (n=18). We generated a random forest model using 18 NK cell genes as predictors of severe PGD with leave-one-out validation. **a)** Receiver operator characteristic curve (ROC) demonstrating the test characteristics of the model. **b)** Relative feature importance of each of the 18 NK cell genes. **c)** Transcript counts of *KLRD1*, the top feature in the model, stratified by PGD status. **d)** Cumulative incidence plot of discharge from the intensive care unit (ICU) for recipients stratified by high BAL *KLRD1* gene transcript counts and PGD status. Box-and-whisker plots display individual data points bound by boxes at the 25th and 75th percentiles and medians depicted with bisecting lines. Comparisons of gene counts were made with the Mann-Whitney U-test. Difference in time to ICU discharge was assessed with a Cox proportional hazards model, displaying log-rank p-value. AUC: area under the ROC curve; HR: hazard ratio.

transcript counts and found that *KLRD1* was increased in BAL from recipients with severe PGD compared to recipients without PGD ($p=0.02$) (figure 1c). We stratified this cohort by PGD status and median of *KLRD1* gene counts from the group without PGD. We found *KLRD1*^{hi} PGD participants had an 8.5-fold increased risk (95% CI 3.2–22.2; $p<0.0001$) for intensive care unit care after transplantation compared to the other participants (figure 1d). These data identify CD94 as a rational target against NK cells that may be exploited to modulate PGD risk.

Mouse pulmonary CD94⁺ NK cells coexpress NKG2A and are activated

CD94 is covalently bonded to NKG2A or NKG2C proteins forming a heterodimeric receptor that recognises non-classical MHC I (HLA-E in humans and Qa-1 in mice) [31]. Because CD94/NKG2A⁺ NK cells in the mouse lung have not been fully characterised, we measured CD94 and NKG2A on cells in the blood, spleen and lung from C57BL/6 mice ($n=6$) (supplementary figure S1). We found that CD94⁺ NK cells had high expression of NKG2A (figure 2a). NKG2A⁺ NK cells comprised nearly 100% of the CD94⁺ population and MFI of CD94 was similar on NK cells in the blood, spleen and lungs of mice (figure 2b and c).

To understand the potential impact of anti-CD94 mAb treatment, we examined immunophenotypes of NKG2A⁺ and NKG2A⁻ NK cells from C57BL/6 mice ($n=10$) in blood, spleen, thoracic lymph nodes and lungs (figure 2d). Across all tissues, NKG2A⁺ NK cells comprised a median (interquartile range (IQR)) 44.8% (42.3–47.8%) of the total NK cell population (figure 2e). CD11b and CD27 are acquired NK cell markers of maturation progressing to CD11b⁺CD27⁻ NK cells (figure 2f). We found that NKG2A⁺ NK cells were immature and had higher expression of CD27 than NKG2A⁻ NK cells (figure 2g–j). We also measured 15 additional markers on lung NK cells (figure 2k). We found no differences in Ly6c, CXCR4, CXCR6, CCR2, Ly49CI or CD69. Notably, in tissues, NKG2A⁺ NK cells had increased CD49a, a marker of tissue residency. DNAM1 and KLRG1, markers of activation, were also increased in the NKG2A⁺ population relative to NKG2A⁻ NK cells. NKG2A⁺ NK cells had increased chemokine receptors (CCR5, CXCR2 and CXCR3) and CD62L, suggesting a circulating source for some of this population. Together, these data suggest that anti-CD94 mAb treatment would target an immature or activated subset of NK cells that comprise roughly half of the pulmonary NK cell niche.

Mouse NKG2A⁺ NK cells are increased, activated and tissue-resident during IRI

To understand the pulmonary NKG2A⁺ NK cell profile during warm IRI (figure 3a), where lungs are not exposed to static cold storage, we investigated differences in the most prevalent markers following HC ($n=7$) and sham ($n=7$) procedures. Overall, the frequency of NKG2A⁺ NK cells was increased in the lung following HC compared to sham thoracotomy ($p=0.04$) (figure 3b). Notably, tissue-resident NKG2A⁺ NK cells were increased in HC lungs compared to sham lungs ($p=0.002$) (figure 3c and d). DNAM1, a marker of NK cell activation, was also increased during lung IRI ($p=0.05$) (figure 3e and f), but no differences were observed in KLRG1 expression (figure 3g and f). These data suggest that IRI leads to a skewed NKG2A⁺ NK cell population described by increased frequencies of tissue-resident and activated cells.

Anti-mouse anti-CD94 treatment reduces lung NK cells

We hypothesised that CD94-based depletion would reduce lung NK cells following warm IRI (figure 4a). To test this hypothesis, we generated an anti-mouse anti-CD94 mAb (supplementary figure S2a–d). This antibody demonstrated high affinity for CD94 antigen (supplementary figure S2e) and high staining of CD94-transduced mouse Ba/F3 cells (supplementary figure S2f).

As expected, anti-mouse anti-CD94 mAb-treated mice had reduced frequencies of lung NK cells compared to isotype-matched control IgG-treated mice ($p=0.004$) and sham mice ($p=0.03$) (figure 4b and c). As the airways and alveoli are primary sites of injury within this model, we examined BAL separately from lung tissue. Absolute BAL NK cells were reduced in the anti-mouse anti-CD94 mAb group when compared to isotype-matched IgG-treated mice ($p=0.04$) (figure 4d). We found no significant differences in the minority of NK cells in the BAL that express CD49a (figure 4e). However, anti-CD94 treatment markedly reduced the overall CD49a⁺ NK cells in the lung ($p=0.001$) (supplementary figure S3a) during IRI. In addition, anti-CD94 treatment reduced the CD49a⁺NKG2A⁺ subsets in the lung (supplementary figure S3b) and BAL (supplementary figure S3c and d). Altogether, these data indicate that anti-CD94 antibodies can effectively penetrate the airway, alveolar and lung tissue compartments.

Other lymphocytes, specifically minor subsets of T-cells, can express NK receptors, including NKG2A [25]. Therefore, we measured the depletion efficiency of CD8⁺ and $\gamma\delta$ T-cells within the lung. We found no differences in depletion in CD8⁺ T-cells ($p=0.3$) (figure 4f) or $\gamma\delta$ T-cells ($p=0.8$) (figure 4g) across the three conditions. We examined NKG2A⁺ populations across all NK cells within the lung (figure 4h). As

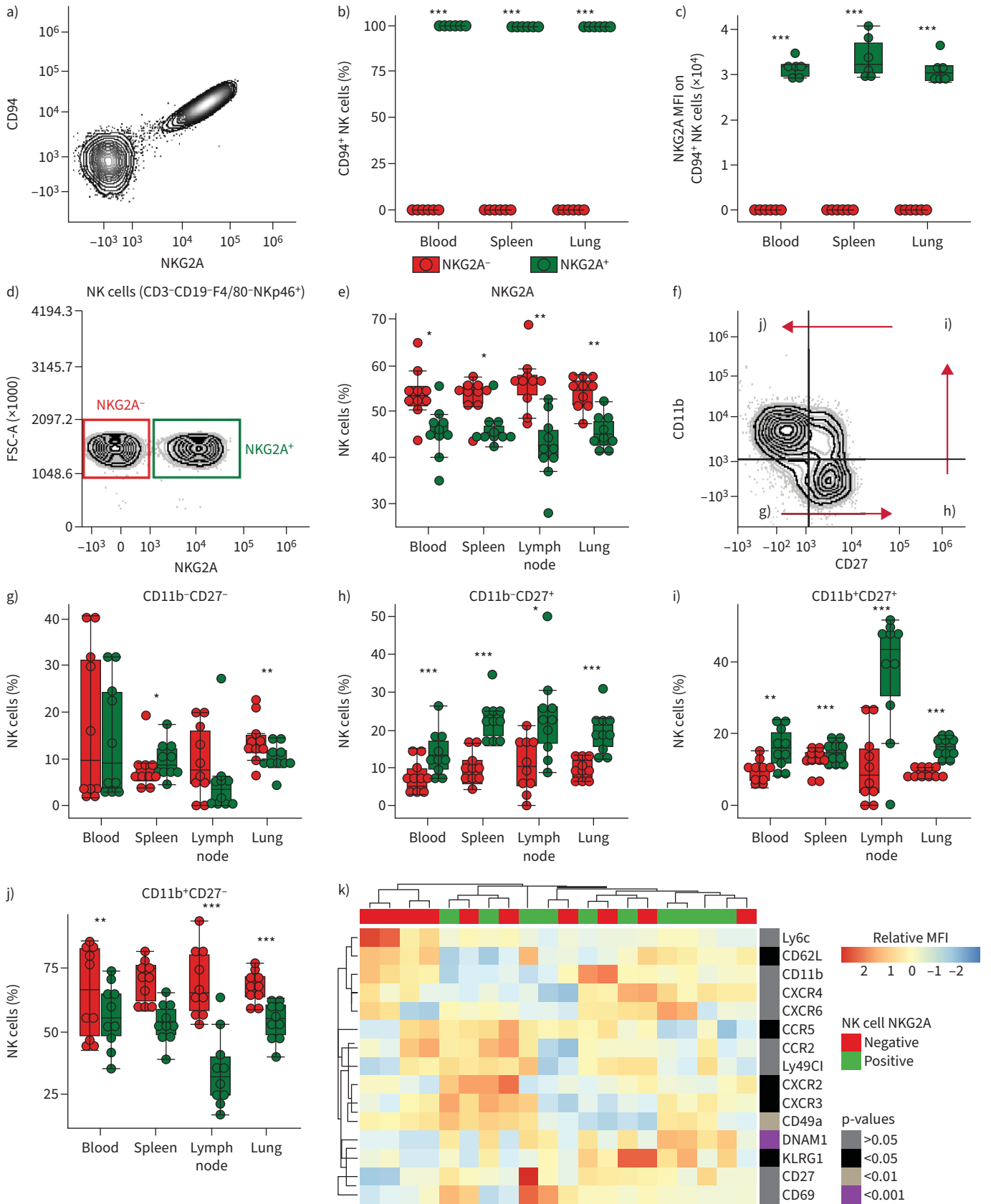


FIGURE 2 Mouse CD94⁺ NKG2A⁺ natural killer (NK) cell profiles. To determine the NK cell expression of CD94 and NKG2A in C57BL/6 mice, several tissues were collected and characterised by spectral flow cytometry. **a)** NK cells (CD3⁻CD19⁻F4/80⁻NKp46⁺) expressing CD94 coexpress NKG2A in a

1:1 ratio. **b)** The percentage of NKG2A expression on CD94⁺ cells is increased across blood, spleen and lung NK cells. **c)** In CD94⁺ NK cells, NKG2A mean fluorescence intensity (MFI) is increased on CD94⁺ NK cells. **d)** Representative contour plots of NKG2A gates. **e)** NKG2A⁺ NK cells constitute 40–50% of the NK cell population in blood, spleen, lymph node and lung. **f)** As indicated by arrow directionality, NK cell maturation is defined by acquisition of CD27, gain of CD11b and finally loss of CD27 [55]. We assessed differences in NKG2A across the four NK cell maturation states: **g)** CD11b⁻CD27⁻, **h)** CD11b⁻CD27⁺, **i)** CD11b⁺CD27⁺ and **j)** CD11b⁺CD27⁻. **k)** We assessed additional activation, chemotaxis and tissue-resident markers, and show differences in MFI in a heatmap. Experiments in **b)** and **c)** studied six mice for each condition and other experiments show 10 mice. Box-and-whisker plots display individual data points bound by boxes at the 25th and 75th percentiles and medians depicted with bisecting lines. Differences were assessed using the Mann–Whitney U-test with Benjamini–Hochberg correction for multiple comparisons and paired testing for comparisons within individual animals. *: p<0.05; **: p<0.01; ***: p<0.001. FSC-A: forward scatter area.

expected, the median (IQR) frequency of NKG2A⁺ NK cells was significantly reduced in the anti-mouse anti-CD94 mAb group (3.5% (2.9–7.7%)) compared to both the isotype-matched IgG-treated (38.2% (34.7–44.2%); p=0.004) and sham groups (45.8% (28.8–47.1%); p=0.004) (figure 4i). We also found that anti-mouse anti-CD94 mAb resulted in reduced NKG2A⁺ lymphocytes compared to the other mice (figure 4j). In summary, these data suggest that anti-mouse anti-CD94 mAb treatment targets most lung NK cells but also the broad population of NKG2A-bearing lymphocytes.

Anti-mouse anti-CD94 treatment blunts lung IRI damage

We previously reported that NK cells mediate pulmonary IRI in mice [13]. Here, we hypothesised that anti-mouse anti-CD94 NK cell depletion would reduce lung damage from warm IRI (figure 5a). Representative HE histopathology (n=5 for each condition) from sham, isotype-matched IgG-treated HC and anti-mouse anti-CD94 mAb-treated HC lungs is shown in figure 5b. We performed qualitative assessments of the histopathology [32]. Relative to sham mice, the lungs from isotype-matched IgG-treated HC mice had diffuse alveolar damage that was abrogated in the anti-mouse anti-CD94-treated HC lungs. Diffuse alveolar damage is characterised by neutrophilic infiltration, alveolar interstitial thickening and pulmonary oedema.

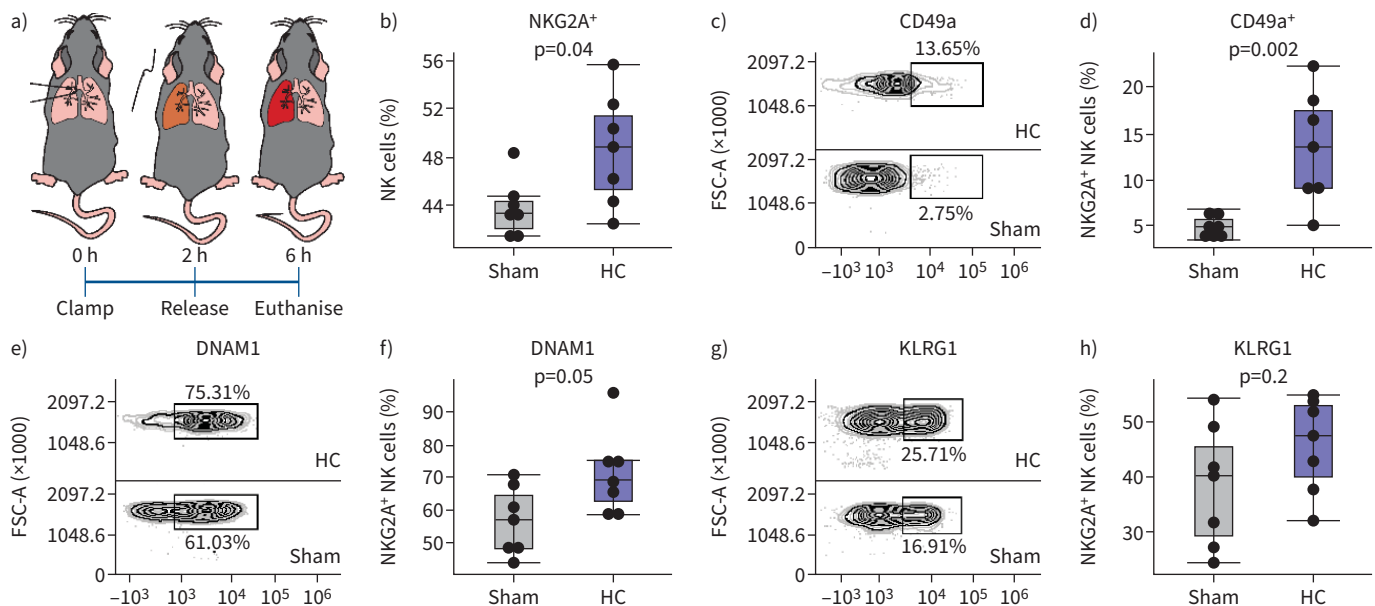


FIGURE 3 NKG2A⁺ natural killer (NK) cells in pulmonary ischaemia-reperfusion injury (IRI). We identified differences during IRI in the NKG2A⁺ populations. **a)** We performed warm IRI with the hilar clamp (HC) model. A slip knot (HC) (n=7) or a sham suture (n=7) was tied around the left hilum and released 2 h later, followed by 4 h of reperfusion before the mice were euthanised. **b)** There was an increase in percentage of NKG2A⁺ NK cells in the lungs following HC. **c)** Representative contour plots of CD49a in NKG2A⁺ NK cells. **d)** CD49a was increased on NKG2A⁺ NK cells in the lung following HC. **e)** Representative contour plots of DNAM1 in NKG2A⁺ NK cells. **f)** Of the NKG2A⁺ NK cell population, lungs that underwent HC have an increased percentage of DNAM1. **g)** Representative contour plots of KLRG1 in NKG2A⁺ NK cells. **h)** There was no difference in expression of KLRG1 between conditions. Experiments studied five mice for each condition. Box-and-whisker plots display individual data points bound by boxes at the 25th and 75th percentiles and medians depicted with bisecting lines. Differences were assessed using the Mann–Whitney U-test with p<0.05 considered significant. FSC-A: forward scatter area.

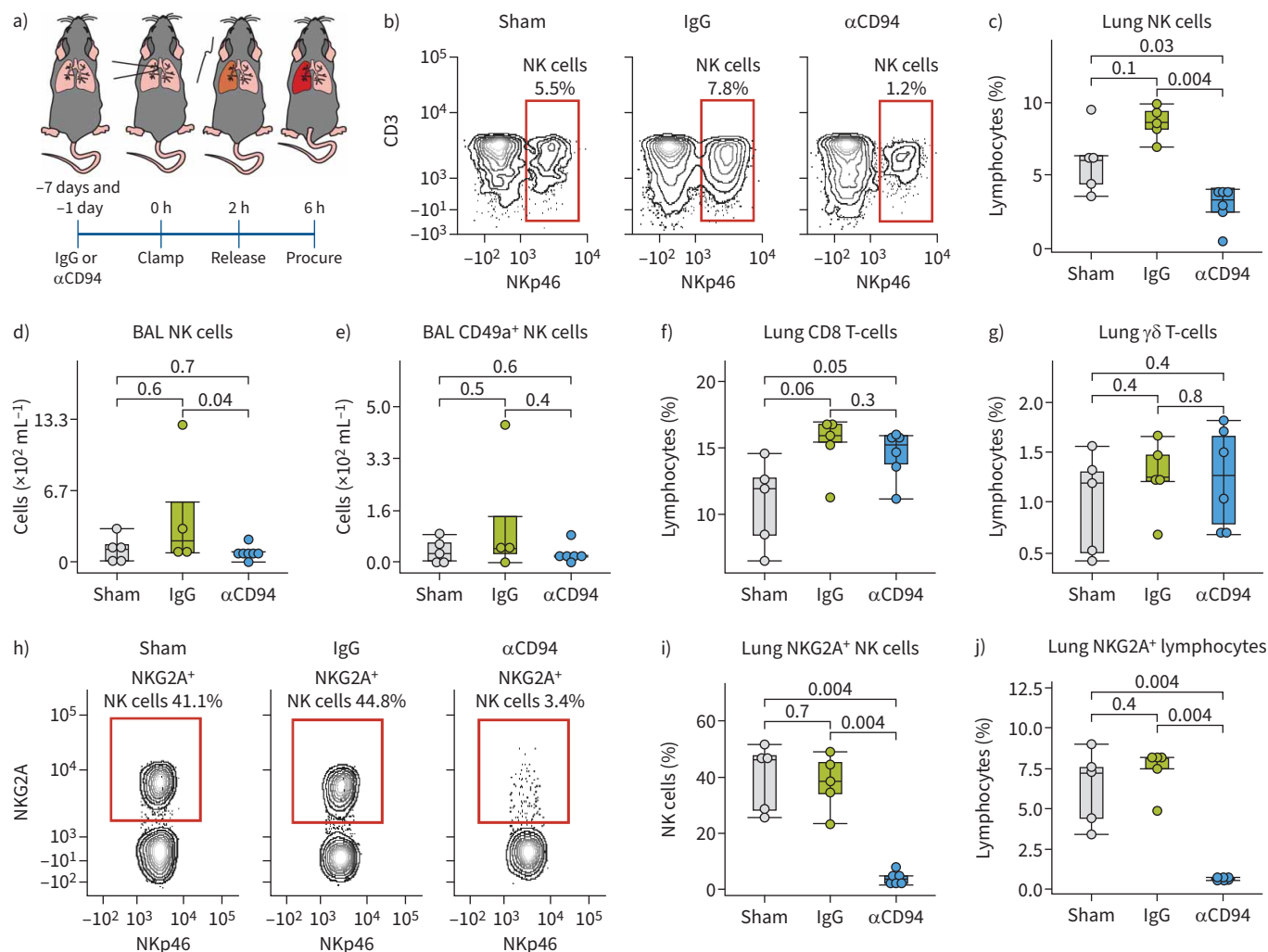


FIGURE 4 Lung and bronchoalveolar lavage (BAL) natural killer (NK) cells are reduced with anti-CD94 treatment. **a**) C57BL/6 mice underwent sham procedures ($n=5$) or were treated with $10 \text{ mg}\cdot\text{kg}^{-1}$ of anti-CD94 antibody (αCD94) ($n=6$) or isotype-matched control IgG ($n=5$) at 7 days and 1 day prior to hilar clamp (HC) procedures. **b**) Representative contour plots of NK cells ($\text{CD3}^-\text{CD19}^-\text{F4/80}^-\text{NKp46}^+$) across conditions. **c**) Percentages of lung NK cells were increased during HC in the isotype-matched IgG-treated group and decreased with anti-CD94 treatment. **d**) Absolute BAL NK cells were reduced with anti-CD94 treatment. **e**) Absolute BAL CD49a^+ NK cells. **f**) CD8^+ T-cells in the lung across the conditions. **g**) Percentage of $\gamma\delta$ T-cells in the lung. **h**) Representative contour plots of NKG2A^+ NK cells in the lung across the three conditions. **i**) Percentage of lung NKG2A^+ NK cells. **j**) Percentage of NKG2A^+ lymphocytes in the lung across the conditions. Box-and-whisker plots display individual data points bound by boxes at the 25th and 75th percentiles and medians depicted with bisecting lines. Differences were assessed using the Mann-Whitney U-test with Benjamini-Hochberg correction for multiple comparisons with $p<0.05$ considered significant.

We quantified lung injury by measuring P_{aO_2} and with radiolabelled ^{125}I -albumin to derive lung extravascular lung water, extravascular plasma equivalents and endothelial permeability. The anti-mouse anti-CD94-treated HC mice had significantly higher median (IQR) P_{aO_2} (462 (439–515) mmHg) relative to isotype-matched IgG-treated HC mice (323 (256–377) mmHg; $p=0.009$) and similar P_{aO_2} to sham-treated mice (622 (592–647) mmHg; $p=0.34$) (figure 5c). We found comparable volumes of extravascular lung water between sham (16.7 (10.8–20.5) μL) and anti-CD94-treated HC mice (24.8 (18.6–28) μL ; $p=0.34$) with increased volumes within the isotype-matched IgG-treated HC mice (33.9 (27.9–44) μL ; $p=0.005$ and $p=0.02$, respectively) (figure 5d). There was a similar pattern of findings between the three groups for extravascular plasma equivalents (figure 5e). Extravasation of albumin was reduced in anti-CD94 HC lungs compared to isotype-matched control Ig-treated HC lungs ($p=0.01$) but was increased relative to sham lungs ($p=0.05$) (figure 5f). Finally, we observed similar findings in endothelial permeability across the three groups (figure 5g). Separately, we found no differences in P_{aO_2} or histology between sham mice treated with anti-CD94 antibody compared to those without antibody (supplementary figure S4).

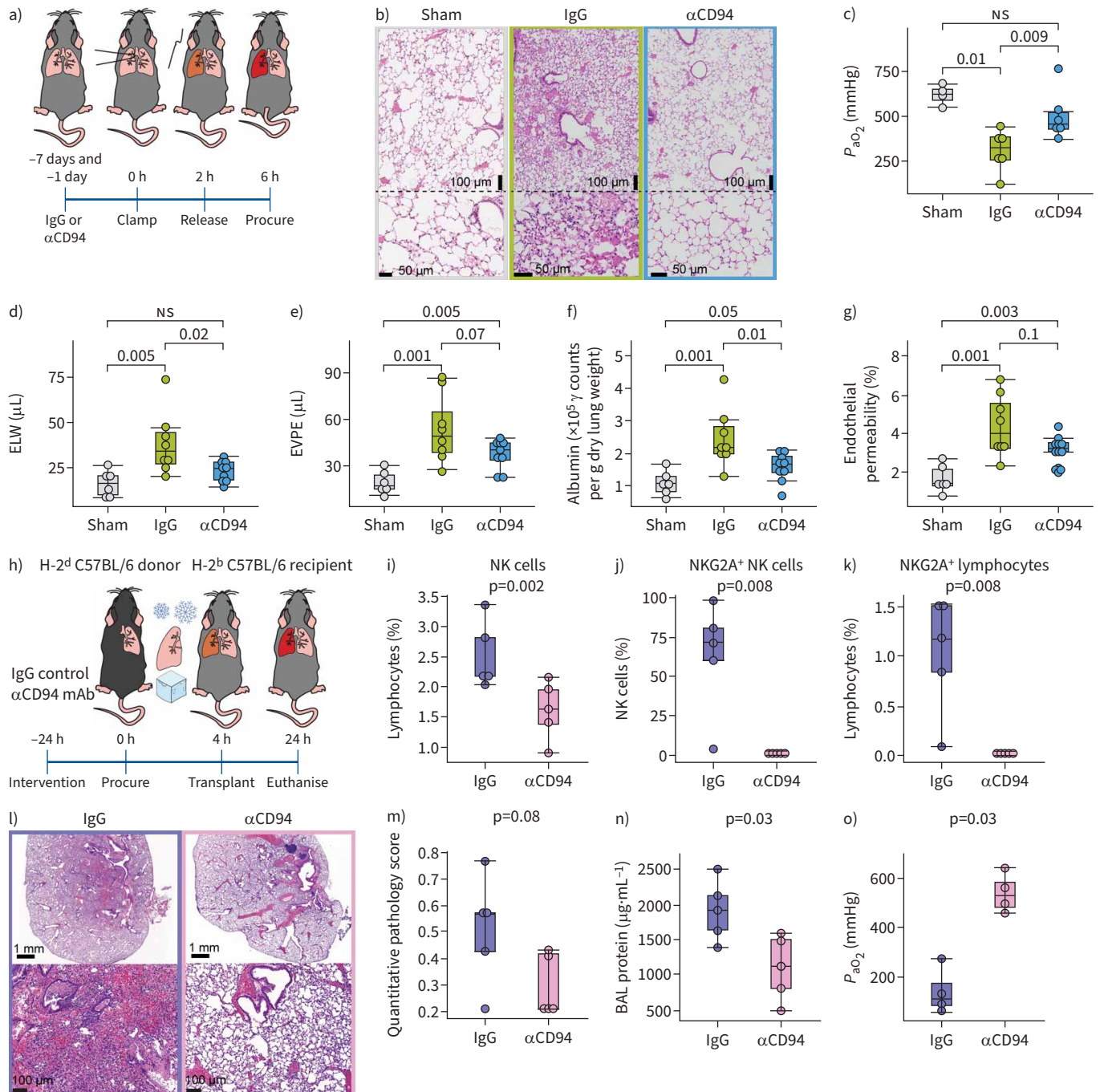


FIGURE 5 CD94-based natural killer (NK) cell depletion reduces lung ischaemia-reperfusion injury. **a)** Mice underwent sham procedures or received intraperitoneal anti-CD94 antibody (α CD94) or isotype-matched control antibody (IgG) 7 days and 1 day preceding hilar clamp. **b)** haematoxylin/eosin (HE) staining of representative lungs ($n=3$ per condition). Quantitative injury metrics were collected for each condition and displayed as **c)** arterial oxygen tension (P_{aO_2}), **d)** extravascular lung water (ELW), **e)** extravascular plasma equivalents (EVPE), **f)** γ counts of ¹²⁵I-albumin per gram of dry lung and **g)** endothelial permeability. P_{aO_2} experiments show sham-treated ($n=5$), IgG ($n=6$) and anti-CD94-treated mice ($n=6$), whereas other metrics display sham-treated ($n=6$), IgG ($n=8$) and anti-CD94-treated mice ($n=9$). **h)** H-2^d C57BL/6 donor and H-2^b C57BL/6 recipient mice were treated with intraperitoneal isotype-matched IgG control antibody ($n=5$) or anti-CD94 antibody ($n=5$) 24 h preceding the donor lung procurement. H-2^d C57BL/6 donor lung was subjected to 4 h of cold ischaemia before orthotopic lung transplant into a C57BL/6 recipient. **i)** NK cells as a percentage of total lymphocytes in the lung were decreased with treatment. **j)** NKG2A⁺ NK cells in the lung were depleted. **k)** NKG2A⁺ lymphocytes in the lung were depleted. **l)** Representative HE staining of representative lungs ($n=5$). We assessed injury *via* **m)** quantitative pathology score, **n)** bronchoalveolar lavage (BAL) protein and **o)** P_{aO_2} . Box-and-whisker plots display individual data points bound by boxes at the 25th and 75th percentiles and medians depicted with bisecting lines. Differences were assessed using the Mann-Whitney U-test with Benjamini-Hochberg correction for multiple comparisons with $p<0.05$ considered significant. mAb: monoclonal antibody.

Unlike the mouse model of HC-induced lung IRI, human lung transplantation is almost always allogeneic. To investigate the effect of anti-CD94 treatment on IRI in allogeneic conditions, we assessed the effect of anti-CD94 *versus* isotype treatment in C57BL/6 (B6, MHC type: H-2^b) recipients given orthotopic lung allografts from H-2^d C57BL/6 (B6.H2^d, MHC type: H-2^d) mice following 4 h of CI (n=5) (figure 5h). Anti-mouse anti-CD94 treatment resulted in effective NK cell depletion relative to isotype control (p=0.02) (figure 5i). NKG2A⁺ NK cells (p=0.008) (figure 5j) and NKG2A⁺ lymphocytes in general (p=0.008) (figure 5k) were efficiently depleted in the anti-mouse anti-CD94-treated group. Injury to the allografts was quantified by assessing quantitative pathology scores, BAL protein content and P_{aO_2} . The anti-mouse anti-CD94-treated transplants had a trend towards lower pathology score (p=0.08) (figures 5l and m), lower BAL protein content (p=0.03) (figure 5n) and higher P_{aO_2} (p=0.03) (figure 5o). Together, data from two mouse models of IRI suggest that CD94-based depletion reduces quantitative and qualitative measures of lung damage after IRI.

Anti-human anti-CD94 therapy reduces human airway cytotoxicity via NK cell depletion

To evaluate the effects of CD94-targeted depletion in humans, we characterised CD94 expression on T-cells and NK cells from lung transplant recipient PBMCs. NK cells and T-cells were enumerated (figure 6a). We observed higher frequency of CD94 expression on NK cells compared to CD45⁺CD3⁺ T-cells (figure 6b). Specifically, only median (IQR) 16.3% (16–29.8%) of the CD8 T-cells were CD94⁺ (p=0.004) (figure 6c), whereas 79% (77–85.7%) of the NK cells were CD94⁺ (p=0.0005) (figure 6d). We surmised that anti-human anti-CD94 treatment of human PBMCs could deplete up to 80% of the human NK cell population.

To understand the specific phenotypes of lung lymphocytes in patients with PGD, we characterised NK cell markers on BAL cells from human lung transplant recipients in the first 2 weeks after transplantation. Baseline characteristics for this cohort are shown in supplementary table S1. BAL NK cells had high frequencies of CD94 expression (median (IQR) 86.7% (77.8–90.5%); p=0.0005) (figure 6e). We stratified NK cells by CD94 and PGD status (figure 6f) and found that BAL CD94^{hi} NK cells from recipients with PGD had increased NKG2D compared to no PGD CD94^{hi} populations (figure 6f and g). We concluded that by using an anti-CD94-targeted depletion strategy, we would also be depleting a majority of the NKG2D⁺ NK cells.

We also investigated CD94 expression on BAL T-cells. Nearly all CD4 T-cells in the BAL lacked CD94 (p<0.0001) (supplementary figure S5a). CD8 T-cells in the BAL had heterogeneous CD94 expression, with nearly equal CD94^{low} (or negative) and CD94^{hi} expression (p=0.3) (supplementary figure S5b). We observed increased NKG2D on CD94^{hi} CD8 T-cells (p=0.8), but little NKG2D expression on CD4 T-cells (supplementary figure S5c). Thus, a CD94-targeted depletion strategy would be expected to deplete CD8 BAL T-cells but largely spare the CD4 T-cell compartment.

We assessed the *in vitro* depletion efficacy of anti-human anti-CD94 mAb in recipient PBMCs relative to isotype-matched control antibody (figure 6h) [33]. Compared to isotype-matched control IgG, PBMCs treated with $>1 \times 10^{-5} \mu\text{g} \cdot \mu\text{L}^{-1}$ of anti-CD94 had reduced frequencies of NK cells (figure 6i and j). Based on the half-maximal effective concentration (EC₅₀) of $1.3 \times 10^{-4} \mu\text{g} \cdot \mu\text{L}^{-1}$, a concentration of $0.1 \mu\text{g} \cdot \mu\text{L}^{-1}$ of anti-CD94 mAb was set as the effective NK cell depletion dose.

We further hypothesised that anti-human anti-CD94 antibody would reduce killing in our *in vitro* cultures employing hypoxic airway epithelial cells to model IRI. Following 24 h of hypoxia (1% O₂) epithelial cells were co-cultured with lung transplant recipient PBMCs pre-treated with anti-CD94 mAb or isotype-matched IgG control (figure 6k). Airway epithelial cells were identified *via* cell tracer and cytotoxicity was determined by viability (supplementary figure S6). There was reduced killing of hypoxic epithelial cells with anti-human anti-CD94 mAb treatment compared to isotype-matched control IgG treatment (p=0.04) (figure 6l and m). These data suggest that anti-human anti-CD94-targeted therapy is effective at reducing airway epithelial killing, a key surrogate of human PGD.

Anti-mouse CD94-targeted depletion did not affect donor APCs in the allogeneic OLT model

NK cells have been shown to enhance lung allograft tolerance in an OLT model of acute and chronic T-cell-mediated rejection *via* selective depletion of donor APCs [34]. It is unknown how NK cell depletion may modulate long-term allogeneic lung allograft outcomes, independently from IRI. We hypothesised that anti-CD94 NK cell depletion would not alter long-term tolerance in an allogeneic OLT model. Therefore, we treated recipient mice with intraperitoneal isotype-matched IgG control antibody (n=5), anti-mouse anti-CD94 antibody (n=4) or IL-15RC (n=4) 1 h preceding BALB/c allogeneic donor OLT-MWI (no IRI) and measured outcomes at 3 days (figure 7a). IL-15RC was used to stimulate NK cells as a positive control. We found that anti-mouse anti-CD94 antibody reduced lung NK cells (p=0.02) (figure 7b), most

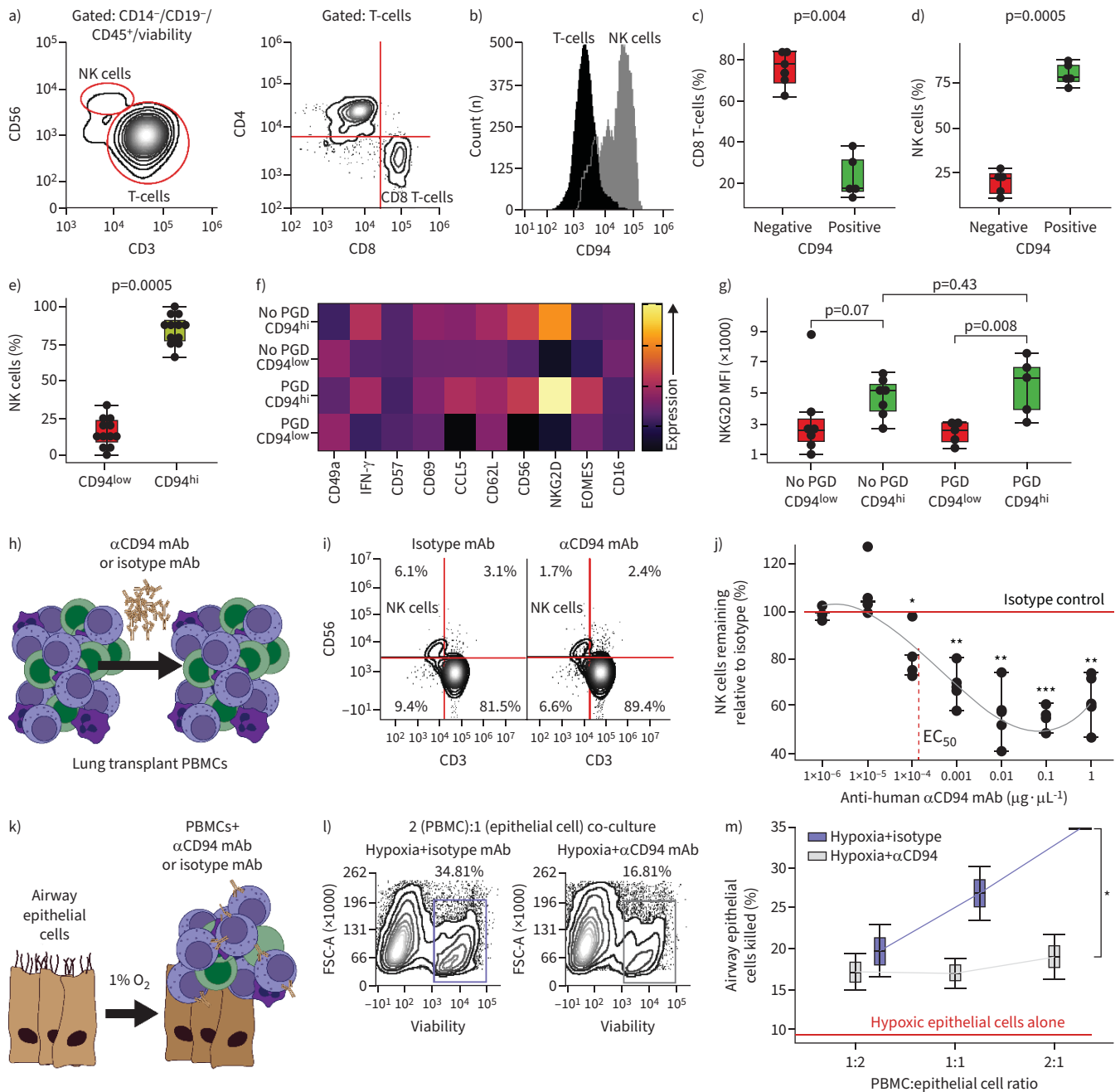


FIGURE 6 Human lung transplant recipient peripheral blood mononuclear cells (PBMCs) treated with anti-CD94 results in natural killer (NK) cell depletion and reduced *in vitro* ischaemia-reperfusion injury. **a)** NK cells and CD4 and CD8 T-cells were quantified with flow cytometry from lung transplant recipient PBMCs (n=5). CD94 was quantified on PBMCs with plots showing **b)** histograms for NK and T-cells, **c)** CD8 T-cells and **d)** NK cells. NK cell CD94 expression was quantified in bronchoalveolar lavage (BAL) from lung transplant recipients with (n=5) and without (n=7) primary graft dysfunction (PGD). **e)** NK cells in the BAL have high frequency of CD94 expression. **f)** Heatmap of NK cell marker mean fluorescence intensity (MFI) differences between CD94^{hi} and CD94^{low} (or negative) NK cells from patients with and without PGD. **g)** Differences in NKG2D MFI values shown by box plots. **h)** *In vitro* depletion of NK cells from lung transplant whole PBMCs was performed. **i)** Representative contour plots from isotype-matched control IgG-treated and anti-CD94 (α CD94)-treated PBMCs treated at 0.1 μ g \cdot μ L⁻¹. **j)** Percentages of NK cells are shown relative to IgG control across different anti-CD94 concentrations. **k)** To assess cytotoxicity, airway epithelial cells were subjected to hypoxia (1% O₂) for 24 h and then co-cultured with PBMCs treated with control IgG or anti-CD94 antibody for an additional 24 h. Airway epithelial cells are stained with CellTrace Violet prior to plating to distinguish PBMCs from epithelial cells during flow cytometry analysis. **l)** Representative contour plots of viability in co-culture across two conditions at 2:1 PBMC:epithelial ratio. **m)** Killing plots of airway epithelial cells across the two conditions. Box-and-whisker plots display individual data points bound by boxes at the 25th and 75th percentiles and medians depicted with bisecting lines. Differences were assessed using the Mann-Whitney U-test. *: p<0.05; **: p<0.01; ***: p<0.001. mAb: monoclonal antibody; EC₅₀: half-maximal effective concentration; FSC-A: forward scatter area.

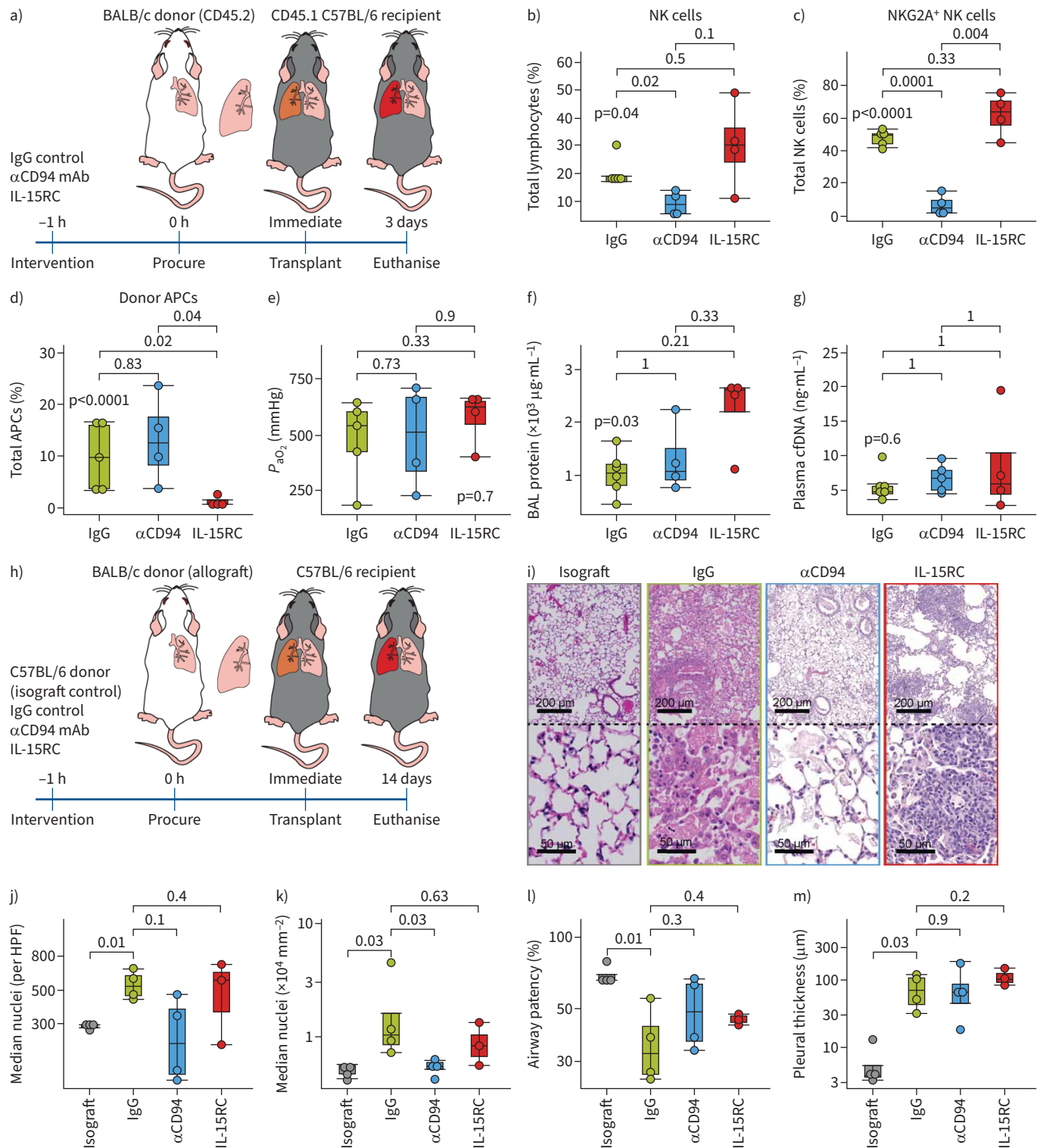


FIGURE 7 CD94-based natural killer (NK) cell depletion in the allogeneic orthotopic lung transplant (OLT) model. **a)** CD45.1 C57BL/6 mice were treated with intraperitoneal isotype-matched IgG control antibody (n=5), anti-CD94 antibody (αCD94) (n=4) or interleukin (IL)-15/IL-15 receptor complex (IL-15RC) (n=4) 1 h preceding OLT with minimal warm ischaemia (OLT-MWI) from a BALB/c donor. We measured lung allograft **b)** total NK cells, **c)** NKG2A⁺ NK cells and **d)** donor antigen-presenting cells (APCs). Injury was quantified by **e)** arterial oxygen tension (P_{aO_2}), **f)** bronchoalveolar lavage (BAL) protein and **g)** plasma cell-free DNA (cfDNA). **h)** We also assessed chronic injury on post-operative day 14 in isografts (n=4) and allograft recipients pre-treated with intraperitoneal isotype-matched IgG control antibody (n=4), anti-CD94 antibody (n=4) or IL-15RC (n=3) 1 h preceding OLT-MWI from a BALB/c donor. **i)** Representative haematoxylin/eosin slide sections from each group. We assessed pathological injury *via*

j) median nuclei per high-powered field (HPF), k) median nuclei surrounding the airways per square millimetre, l) airway patency and m) pleural thickness. Box-and-whisker plots display individual data points bound by boxes at the 25th and 75th percentiles and medians depicted with bisecting lines. Comparisons across experimental groups were made with the Kruskal–Wallis test. Differences were assessed using the Mann–Whitney U-test with Benjamini–Hochberg correction for multiple comparisons with $p < 0.05$ considered significant.

profoundly in the NKG2A⁺ population ($p=0.0001$) (figure 7c) relative to isotype-matched IgG treatment. As expected, we found reduced donor APCs in IL-15RC mice compared to isotype-matched IgG-treated mice ($p=0.02$) (figure 7d). Anti-mouse anti-CD94 antibody had no impact on donor APCs relative to control ($p=0.83$). We observed no differences in P_{aO_2} (figure 7e), BAL protein (figure 7f) or cell-free DNA (figure 7g) across the three groups.

NK cell depletion in a mouse allogeneic OLT model does not alter graft acceptance

In addition to a role in allograft tolerance, NK cells have also been shown to mediate obliterative airway disease in an allogeneic heterotopic tracheal transplant model in an NKG2D-dependent fashion [35]. It is unknown how NK cell depletion would alter lung pathology in the allogeneic OLT model as tracheas lack the complexity of the lung. Therefore, we assessed four different histopathology measures 14 days following transplantation of an untreated isograft or allografts treated with isotype-matched IgG control antibody, anti-mouse anti-CD94-based depletion or IL-15RC (figure 7h). Representative HE images are shown in figure 7i and supplementary figure S7. We found that IgG-treated lungs had increased inflammation by nuclei counted per high-powered field ($p=0.01$) (figure 7j) and surrounding airways ($p=0.03$) (figure 7k) relative to isografts. There was also reduced airway patency ($p=0.01$) (figure 7l) and increased pleural thickness in the control IgG-treated lungs ($p=0.03$) (figure 7m) relative to isografts. Notably, anti-mouse anti-CD94 mAb treatment blunted inflammation around airways relative to IgG-treated mice ($p=0.03$) and IL-15RC had no impact on any of these measures. Together, these suggest a trend to reduced chronic inflammation with NK cell depletion.

Discussion

Here, we describe a novel approach to target an important innate immune cell implicated in the pathogenesis of pulmonary IRI. We show that CD94 is abundant on mouse and human NK cells, and that a mAb efficiently depletes >50% of lung NK cells in the mouse. In mouse and human experimental models, we find that CD94 depletion is effective at reducing lung injury and airway epithelial cell killing, respectively. These findings represent a critical step towards clinical NK cell depletion.

There are key differences in NK cell receptor repertoires between mice and humans. Although both species express CD94, it is expressed on ~50% of mouse NK cells, while it is found on most human NK cells as a bimodal population of CD94^{dim} and CD94^{bright} [36–38]. This explains the ~50% depletion efficiency we observed in the mouse. Compared to historical published data, anti-NK1.1-based treatment resulted in almost complete NK cell depletion due to expression of NK1.1 on all mouse NK cells and, concordantly, achieved nearly twice the reduction in injury relative to our observations here [13]. Nonetheless, we observed clinically significant reductions in mouse lung injury with CD94 depletion. In humans, we found nearly 80% of lung transplant recipient circulating and BAL NK cells expressed CD94 and would expect a greater reduction in NK cells with *in vivo* depletions compared to the mouse. NK cell *in vitro* depletions could potentially be limited by reduced sources of cytokines and viability of cells due to cryopreservation, resulting in diminished antibody-dependent cell-mediated cytotoxicity.

NK cell depletion, rather than receptor blockade, may carry broader repercussions as NK cells participate in a variety of other mechanisms that may impact lung transplant outcomes. Our observations that CD94⁺ NK cells in the BAL of recipients with PGD have increased NKG2D receptor expression suggest that CD94-based depletion may preferentially target this critical subpopulation of NK cells. Consequently, in skin and lung, NK cells have been shown to support early allograft acceptance *via* selective depletion of donor APCs [34, 39]. It was unknown if one-time NK cell depletion at induction would alter this effect. Here, we find that while NK cell stimulation *via* IL-15RC augments donor APC killing, CD94-based depletion had no impact on donor APCs relative to control animals, likely because half of the NK cells were depleted. We also found no detrimental effect of NK cell depletion on chronic graft injury, suggesting that selective depletion of CD94 subsets does not impact this APC-dependent tolerance mechanism. Notably, NK cells play a central role in mitigating human and mouse cytomegalovirus (CMV) infection [40–43]. However, we previously reported that the CMV-specific NK cell populations bearing NKG2C receptors may be deleterious following lung transplantation [44]. NK cells may also mediate

chronic lung allograft dysfunction through NKG2D-mediated recognition of stress molecules on small airway cells [35]. Finally, NK cells are key mediators of antibody-mediated transplant rejection via antibody-dependent cell-mediated cytotoxicity [45–48]. While we have shown that selective CD94-based NK cell depletion blunts acute injury following ischaemia–reperfusion with minimal impact on tolerance, further work is required to determine if depletion may impact these other important end-points.

A particular strength of this study is the concordance of findings within two established mouse models of IRI and in an *in vitro* human model of airway cell killing. In addition, we modelled and replicated an important mechanism of NK cell tolerance and demonstrated no large differences in long-term outcomes with CD94-based NK cell depletion versus positive and negative control conditions. Another important limitation is that the *in vitro* human model of airway cell killing used recipient cells from the circulation rather than BAL as there are too few lymphocytes in these samples for these experiments. While tissue-specific functional differences may be unaccounted for in this study, we previously reported that most NK cells responding to lung IRI are from the circulation [13]. This study focused on NK cells, but CD94 is expressed in lower frequencies on T-cells [49]. As such, the results observed from CD94-based depletion may not be due to impacts on NK cell populations alone.

These findings have broad implications outside of lung transplantation. Notably, existing studies have identified NK cells and hypoxia signalling as important transcriptional pathways in acute respiratory distress syndrome patients with bacterial lower respiratory infections [50, 51]. In kidney IRI, NK cells have also been shown to mediate damage through NKG2D activation [52–54]. Together, these data suggest that CD94-based depletion strategies may be beneficial in other acute injury syndromes.

In conclusion, we describe a novel and efficacious approach to deplete NK cells prior to pulmonary IRI. These findings represent a critical intermediary step to a human trial of CD94-based NK cell depletion in lung transplantation to prevent PGD. Such a strategy may rationally be included in induction therapy.

Acknowledgements: We thank the UCSF transplant pulmonologists Jeff Golden, Mary Ellen Kleinhenz, Lorianna Leard, Rupal Shah, Nicholas Kolaitis, Aida Venado and the other members of the clinical lung transplant team for their care of our patients and design of the clinical protocols. We thank Fengchun Liu of the UCSF Microvascular Surgery Core for his work on the hilar clamp model system. We are thankful for the cooperation of Donor Network West, for all the organ and tissue donors, and their families for giving gifts of life and knowledge with their generous donation.

Ethics statement: Our study was conducted under approved protocols from our animal and human research committees. Written informed consent was obtained from all participants prior to inclusion in the study. All animal procedures and experiments were conducted according to protocols approved by the UCSF Institutional Animal Care Use Committee.

Author contributions: Conceptualisation: D.R. Calabrese, L.L. Lanier, J.R. Greenland, R. Shi, J. Richardson. Methodology: D.R. Calabrese, T. Tsao, L. Bai, S.J. Cleary. Investigation: D.R. Calabrese, T. Tsao, L. Qiu, A. Shemesh, A.M. Hernandez, L. Bai, R. Bharti, J.P. Singer, J. Kukreja, J. Kang, A. Salles, T. Sputova, S.J. Cleary, N.Y. Greenland, D. Zhang. Data Analysis: D.R. Calabrese, T. Tsao, K. Dilley, R. Shi, R. Bharti, N.Y. Greenland. Visualisation: D.R. Calabrese. Funding acquisition: D.R. Calabrese, M.R. Looney, J.P. Singer. Writing (original draft): D.R. Calabrese. Writing (review and editing): D.R. Calabrese, S.R. Hays, L.L. Lanier, J.R. Greenland, M.R. Looney, J.P. Singer, R. Shi, J. Santos, K. Dilley, M. Will, N. Tomasevic, T. Tsao.

Conflict of interest: R. Shi, L. Bai, K. Dilley, M. Will, N. Tomasevic, T. Sputova, A. Salles and J. Kang are employees and shareholders of Dren Bio, Inc. N. Tomasevic is a founder and holds a management position at Dren Bio, Inc. M. Will holds a management position at Dren Bio, Inc. L.L. Lanier is a consultant for Dren Bio, Inc. The authors have no additional conflicts of interest to disclose.

Support statement: The authors report partial project funding with support from Dren Bio. D.R. Calabrese receives salary support from the CFF (CALABR19Q0) and VA ORD BLRD (1K2BX005301). J.R. Greenland receives salary support from the CFF, VA ORD (CX002011) and NIH (HL151552). L.L. Lanier is supported by the Parker Institute for Cancer Immunotherapy (PICI) and the NIH (AI068129). M.R. Looney and J.P. Singer were supported by the NIH (R01HL130324) and M.R. Looney was supported by the NIH (R35HL161241). We acknowledge the Parnassus Flow Cytometry Core (RRID:SCR 018206) supported in part by NIH P30DK063720 and by NIH S10 Instrumentation Grant S10 1S10OD026940-01. The animal microsurgery core was also supported by the Nina Ireland Program for Lung Health. Funding information for this article has been deposited with the Crossref Funder Registry.

References

- 1 Valapour M, Lehr CJ, Schladt DP, et al. OPTN/SRTR 2021 annual data report: lung. *Am J Transplant* 2023; 23: Suppl. 1, S379–S442.
- 2 Diamond JM, Lee JC, Kawut SM, et al. Clinical risk factors for primary graft dysfunction after lung transplantation. *Am J Respir Crit Care Med* 2013; 187: 527–534.
- 3 Snell GI, Yusef RD, Weill D, et al. Report of the ISHLT Working Group on Primary Lung Graft Dysfunction, part I: Definition and grading – A 2016 Consensus Group Statement of the International Society for Heart and Lung Transplantation. *J Heart Lung Transplant* 2017; 36: 1097–1103.
- 4 Kolaitis NA, Gao Y, Soong A, et al. Primary graft dysfunction attenuates improvements in health-related quality of life after lung transplantation, but not disability or depression. *Am J Transplant* 2021; 21: 815–824.
- 5 Paraskeva MA, Borg BM, Paul E, et al. Abnormal one-year post-lung transplant spirometry is a significant predictor of increased mortality and chronic lung allograft dysfunction. *J Heart Lung Transplant* 2021; 40: 1649–1657.
- 6 Li D, Weinkauff J, Kapasi A, et al. Baseline lung allograft dysfunction in primary graft dysfunction survivors after lung transplantation. *Respir Med* 2021; 188: 106617.
- 7 Morrison MI, Pither TL, Fisher AJ. Pathophysiology and classification of primary graft dysfunction after lung transplantation. *J Thorac Dis* 2017; 9: 4084–4097.
- 8 Cantu E, Diamond JM, Cevasco M, et al. Contemporary trends in PGD incidence, outcomes, and therapies. *J Heart Lung Transplant* 2022; 41: 1839–1849.
- 9 Bharat A, Kreisel D. Immunopathogenesis of primary graft dysfunction after lung transplantation. *Ann Thorac Surg* 2018; 105: 671–674.
- 10 Calabrese DR, Lanier LL, Greenland JR. Natural killer cells in lung transplantation. *Thorax* 2019; 74: 397–404.
- 11 Kumar S. Natural killer cell cytotoxicity and its regulation by inhibitory receptors. *Immunology* 2018; 154: 383–393.
- 12 Calabrese DR, Tsao T, Magnen M, et al. NKG2D receptor activation drives primary graft dysfunction severity and poor lung transplantation outcomes. *JCI Insight* 2022; 7: e164603.
- 13 Calabrese DR, Aminian E, Mallavia B, et al. Natural killer cells activated through NKG2D mediate lung ischemia-reperfusion injury. *J Clin Invest* 2021; 131: e137047.
- 14 Aguilar OA, Qualls AE, Gonzalez-Hinojosa MDR, et al. MICB genomic variant is associated with NKG2D-mediated acute lung injury and death. *Am J Respir Crit Care Med* 2024; 209: 70–82.
- 15 Chandrashekar S, Crow Pharm SA, Shah SZ, et al. Immunosuppression for lung transplantation: current and future. *Curr Transplant Rep* 2018; 5: 212–219.
- 16 Shagabayeva L, Osho AA, Moonsamy P, et al. Induction therapy in lung transplantation: a contemporary analysis of trends and outcomes. *Clin Transplant* 2022; 36: e14782.
- 17 Meehan AC, Mifsud NA, Nguyen TH, et al. Impact of commonly used transplant immunosuppressive drugs on human NK cell function is dependent upon stimulation condition. *PLoS One* 2013; 8: e60144.
- 18 Martin JF, Perry JS, Jakhete NR, et al. An IL-2 paradox: blocking CD25 on T cells induces IL-2-driven activation of CD56^{bright} NK cells. *J Immunol* 2010; 185: 1311–1320.
- 19 Groetzner J, Kur F, Spelsberg F, et al. Airway anastomosis complications in *de novo* lung transplantation with sirolimus-based immunosuppression. *J Heart Lung Transplant* 2004; 23: 632–638.
- 20 Shemesh A, Su Y, Calabrese DR, et al. Diminished cell proliferation promotes natural killer cell adaptive-like phenotype by limiting FcεR1 expression. *J Exp Med* 2022; 219: e20220551.
- 21 Abel AM, Yang C, Thakar MS, et al. Natural killer cells: development, maturation, and clinical utilization. *Front Immunol* 2018; 9: 1869.
- 22 Ryan JC, Turck J, Niemi EC, et al. Molecular cloning of the NK1.1 antigen, a member of the NKR-P1 family of natural killer cell activation molecules. *J Immunol* 1992; 149: 1631–1635.
- 23 Vadstrup K, Bendtsen F. Anti-NKG2D mAb: a new treatment for Crohn's disease? *Int J Mol Sci* 2017; 18: 1997.
- 24 Cleary SJ, Kwaan N, Tian JJ, et al. Complement activation on endothelium initiates antibody-mediated acute lung injury. *J Clin Invest* 2020; 130: 5909–5923.
- 25 Santos J, Wang P, Shemesh A, et al. CCR5 drives NK cell-associated airway damage in pulmonary ischemia-reperfusion injury. *JCI Insight* 2023; 8: e173716.
- 26 Sayah DM, Mallavia B, Liu F, et al. Neutrophil extracellular traps are pathogenic in primary graft dysfunction after lung transplantation. *Am J Respir Crit Care Med* 2015; 191: 455–463.
- 27 Krupnick AS, Lin X, Li W, et al. Orthotopic mouse lung transplantation as experimental methodology to study transplant and tumor biology. *Nat Protoc* 2009; 4: 86–93.
- 28 Folkesson HG, Matthay MA, Hébert CA, et al. Acid aspiration-induced lung injury in rabbits is mediated by interleukin-8-dependent mechanisms. *J Clin Invest* 1995; 96: 107–116.
- 29 Wiener-Kronish JP, Albertine KH, Matthay MA. Differential responses of the endothelial and epithelial barriers of the lung in sheep to *Escherichia coli* endotoxin. *J Clin Invest* 1991; 88: 864–875.
- 30 Schneider CA, Rasband WS, Eliceiri KW. NIH Image to ImageJ: 25 years of image analysis. *Nat Method* 2012; 9: 671–675.

- 31 Iwaszko M, Bogunia-Kubik K. Clinical significance of the HLA-E and CD94/NKG2 interaction. *Arch Immunol Ther Exp* 2011; 59: 353–367.
- 32 Matute-Bello G, Downey G, Moore BB, et al. An official American Thoracic Society workshop report: features and measurements of experimental acute lung injury in animals. *Am J Respir Cell Mol Biol* 2011; 44: 725–738.
- 33 Shi K, Tan C, Bai L, et al. DR-01, a non-fucosylated anti-CD94 antibody, depletes leukemic cells in *ex vivo* and *in vivo* models of large granular lymphocyte leukemia. *Blood* 2022; 140: Suppl. 1, 2259–2260.
- 34 Jungraithmayr W, Codarri L, Bouchaud G, et al. Cytokine complex-expanded natural killer cells improve allogeneic lung transplant function *via* depletion of donor dendritic cells. *Am J Respir Crit Care Med* 2013; 187: 1349–1359.
- 35 Kawakami T, Ito K, Matsuda Y, et al. Cytotoxicity of natural killer cells activated through NKG2D contributes to the development of bronchiolitis obliterans in a murine heterotopic tracheal transplant model. *Am J Transplant* 2017; 17: 2338–2349.
- 36 Borrego F, Masilamani M, Marusina AI, et al. The CD94/NKG2 family of receptors. *Immunol Res* 2006; 35: 263–277.
- 37 Yu J, Mao HC, Wei M, et al. CD94 surface density identifies a functional intermediary between the CD56^{bright} and CD56^{dim} human NK-cell subsets. *Blood* 2010; 115: 274–281.
- 38 Fang M, Orr MT, Spee P, et al. CD94 is essential for NK cell-mediated resistance to a lethal viral disease. *Immunity* 2011; 34: 579–589.
- 39 Yu G, Xu X, Vu MD, et al. NK cells promote transplant tolerance by killing donor antigen-presenting cells. *J Exp Med* 2006; 203: 1851–1858.
- 40 Adams NM, Geary CD, Santosa EK, et al. Cytomegalovirus infection drives avidity selection of natural killer cells. *Immunity* 2019; 50: 1381–1390.
- 41 Bayard C, Lepetitcorps H, Roux A, et al. Coordinated expansion of both memory T cells and NK cells in response to CMV infection in humans. *Eur J Immunol* 2016; 46: 1168–1179.
- 42 Daniels KA, Devora G, Lai WC, et al. Murine cytomegalovirus is regulated by a discrete subset of natural killer cells reactive with monoclonal antibody to Ly49H. *J Exp Med* 2001; 194: 29–44.
- 43 Lopez-Verges S, Milush JM, Schwartz BS, et al. Expansion of a unique CD57⁺NKG2C^{hi} natural killer cell subset during acute human cytomegalovirus infection. *Proc Natl Acad Sci USA* 2011; 108: 14725–14732.
- 44 Calabrese DR, Chong T, Wang A, et al. NKG2C natural killer cells in bronchoalveolar lavage are associated with cytomegalovirus viremia and poor outcomes in lung allograft recipients. *Transplantation* 2019; 103: 493–501.
- 45 Calabrese DR, Chong T, Singer JP, et al. CD16⁺ natural killer cells in bronchoalveolar lavage are associated with antibody-mediated rejection and chronic lung allograft dysfunction. *Am J Transplant* 2023; 23: 37–44.
- 46 Loupy A, Van Huyen JPD, Hidalgo L, et al. Gene expression profiling for the identification and classification of antibody-mediated heart rejection. *Circulation* 2017; 135: 917–935.
- 47 Parkes MD, Halloran PF, Hidalgo LG. Evidence for CD16a-mediated NK cell stimulation in antibody-mediated kidney transplant rejection. *Transplantation* 2017; 101: e102–e111.
- 48 Toyoda M, Ge S, Suviolahti E, et al. IFN γ production by NK cells from HLA-sensitized patients after *in vitro* exposure to allo-antigens. *Transpl Immunol* 2012; 26: 107–112.
- 49 Arlettaz L, Villard J, de Rham C, et al. Activating CD94:NKG2C and inhibitory CD94:NKG2A receptors are expressed by distinct subsets of committed CD8⁺ TCR alpha β lymphocytes. *Eur J Immunol* 2004; 34: 3456–3464.
- 50 Sarma A, Christenson SA, Byrne A, et al. Tracheal aspirate RNA sequencing identifies distinct immunological features of COVID-19 ARDS. *Nat Commun* 2021; 12: 5152.
- 51 Wesselkamper SC, Eppert BL, Motz GT, et al. NKG2D is critical for NK cell activation in host defense against *Pseudomonas aeruginosa* respiratory infection. *J Immunol* 2008; 181: 5481–5489.
- 52 Feng L, Cheng F, Ye Z, et al. The effect of renal ischemia-reperfusion injury on expression of RAE-1 and H60 in mice kidney. *Transplant Proc* 2006; 38: 2195–2198.
- 53 Suarez-Alvarez B, Fernandez-Sanchez A, Lopez-Vazquez A, et al. NKG2D and its ligands: active factors in the outcome of solid organ transplantation? *Kidney Int Suppl* 2011; 1: 52–57.
- 54 Victorino F, Sojka DK, Brodsky KS, et al. Tissue-resident NK cells mediate ischemic kidney injury and are not depleted by anti-asialo-GM1 antibody. *J Immunol* 2015; 195: 4973–4985.
- 55 Chiossone L, Chaix J, Fuseri N, et al. Maturation of mouse NK cells is a 4-stage developmental program. *Blood* 2009; 113: 5488–5496.